

# Learned Gradient of a Regularizer for Plug-and-Play Gradient Descent \*

Rita Fermanian<sup>†</sup>, Mikael Le Pendu<sup>†</sup>, and Christine Guillemot<sup>†</sup>

**Abstract.** The Plug-and-Play (PnP) framework allows integrating advanced image denoising priors into optimization algorithms, to efficiently solve a variety of image restoration tasks. The Plug-and-Play alternating direction method of multipliers (ADMM) and the Regularization by Denoising (RED) algorithms are two examples of such methods that made a breakthrough in image restoration. However, while the former method only applies to proximal algorithms, it has recently been shown that there exists no regularization that explains the RED algorithm when the denoisers lack Jacobian symmetry, which happen to be the case of most practical denoisers. To the best of our knowledge, there exists no method for training a network that directly represents the gradient of a regularizer, which can be directly used in Plug-and-Play gradient-based algorithms. We show that it is possible to train a denoiser along with a network that corresponds to the gradient of its regularizer. We use this gradient of the regularizer in gradient-based optimization methods and obtain better results comparing to other generic Plug-and-Play approaches. We also show that the regularizer can be used as a pre-trained network for unrolled gradient descent. Lastly, we show that the resulting denoiser allows for a quick convergence of the Plug-and-Play ADMM.

**Key words.** Inverse problems, Regularization, Plug-and-Play Prior, Gradient Descent

**MSC codes.** 62H35, 68U10, 94A08,68T99

**1. Introduction.** This paper proposes a new approach for solving linear inverse problems in imaging. Inverse problems represent the task of reconstructing an unknown signal from a set of corrupted observations. Examples of inverse problems are denoising, super-resolution, deblurring and inpainting, which all are restoration problems. Supposing that the degradation process is known, we can formulate the restoration task as the minimization of a data fidelity term. However, inverse problems are ill-posed. Hence they do not have a unique solution. A common approach for dealing with this issue consists in introducing prior knowledge on images, in the form of an extra regularization term which penalizes unlikely solutions in the optimization problem. Early methods used handcrafted priors such as total variation (TV) [4,5,25,34] and wavelet regularizers [13], as well as low-rank regularizers such as weighted Schatten [23,42] and nuclear [16,17] norms of local image features.

With the advancement of deep learning, problem-specific deep-neural networks yielded a significant performance improvement in the field of image restoration. In fact, using a reasonable amount of training data, we can train a neural network that can learn a mapping between the space of measurements (i.e. degraded images) and the corresponding solution space (i.e. ground-truth images). These networks interpreted as deep regression models are efficient for solving different applications such as sparse signal recovery [28], deconvolution and deblurring [11,12,38,39,43], super-resolution [10,22,29], and demosaicing [19]. Nevertheless, they have to be designed specifically for each application, hence they lack genericity and

---

\*This work was supported by the french ANR research agency in the context of the artificial intelligence project DeepCIM.

<sup>†</sup>Inria Rennes – Bretagne-Atlantique, 263 Avenue Général Leclerc, 35042 Rennes Cedex, France (e-mail: first-name.lastname@inria.fr)

interpretability.

Recent methods have been introduced with the goal of coupling classical optimization with deep learning techniques. Most of these methods are derived from the idea of the Plug-and-Play prior (PnP) popularized by Venkatakrisnan et al. [41]. The method in [41] uses the ADMM algorithm [2] which iteratively and alternately solves two sub-problems, each associated to either the regularization term or the data fidelity term. The authors have noted that the regularization sub-problem (formally defined as the proximal operator of the regularization term) can be advantageously replaced by applying a state-of-the-art denoiser, hence removing the need for explicitly defining a regularization term. While early works [6, 36, 41] used traditional denoising methods such as BM3D [8] or non-local means [3], the approach makes it possible to leverage the high performances of deep neural networks for solving various tasks with a single deep denoiser [31, 46, 47].

However, these methods remain limited to proximal algorithms which make use of the proximal operator of the regularization term, but they do not apply to the simple gradient descent algorithm which instead requires the gradient of the regularization term with respect to the current estimate. For this reason, despite the growing interest for Plug-and-Play algorithms, as well as the extensive use of gradient descent in machine learning, the Plug-and-Play gradient descent has seldom been studied in the literature.

To the best of our knowledge, the only method which intends to model the gradient of a regularizer for solving inverse problems in a similar Plug-and-Play context, is the Regularization by Denoising (RED) proposed by Romano et al. [32]. Using an off-the-shelf denoiser, the RED method explicitly defines a regularization term which is proportional to the inner product between the unknown image and the residual of its denoising. They also show that, under certain conditions, the gradient of this regularization term is the denoising residual itself. However, Reehorst and Schniter [30] proved later that the gradient expression proposed in RED is not justified with denoisers that lack Jacobian symmetry, which excludes most practical denoisers such as BM3D [8] or state-of-the-art deep neural networks. Moreover, although the regularization term is explicitly defined in RED, it depends on the noise level parameter of the denoiser used. This involves an additional hyper-parameter that must be tuned per-application, whereas theoretically, a regularizer (and thus its gradient) should fully determine the image prior, regardless of the task to be solved.

It must also be noted that a network playing the role of the gradient of a regularizer can be trained in the context of the so-called “unrolled algorithms” [9, 14, 15, 21, 27, 29, 35, 37, 44]. Extending on the Plug-and-Play idea, this approach consists in training the regularizing network in an end-to-end fashion so that applying a given number of iterations of the algorithm yields the best results for a specific inverse problem. In particular, the Total Deep Variation (TDV) method [21] consists of an unrolled gradient based algorithm where the network represents the regularization function. Due to the end-to-end training, high quality results can be obtained for the targeted application. However, the approach loses the genericity of Plug-and-Play algorithms. Furthermore, it is not clear what interpretation can be given to the trained network which does not only learn prior knowledge on images, but also task-specific features.

The aim of this paper is then to train a network that mathematically represents the gradient of a regularizer, without relying on task-specific training. Hence, our regularizing

network can be used for solving inverse problems using a simple gradient descent algorithm, unlike existing Plug-and-Play methods that are suitable only for proximal algorithms. Our method makes use of a second network pre-trained for the denoising task. Based on the assumption that the denoiser represents the proximal operator of an underlying differentiable regularizer (defining the image prior), we derive a loss function that links the denoiser and the regularizer’s gradient networks. However, since there is no guarantee that this assumption is mathematically valid for a denoising neural network, we propose an approach where the pre-trained denoiser is modified jointly with the training of our regularizer’s gradient network. This approach encourages the denoiser to be consistent with the definition of a proximal operator of a differentiable regularizer, and significantly improves our results in comparison to keeping the denoiser fixed.

We use our network to solve different inverse problems such as super-resolution, deblurring and pixel-wise inpainting in a simple gradient based algorithm, and obtain better results when comparing to other generic methods. We also show that our training method can advantageously serve as a pre-training stage, later facilitating a per-application tuning of the regularization network in the framework of unrolled gradient descent.

**2. Notations and problem statement.** We consider the linear inverse problem which consists in recovering an image  $x \in \mathbb{R}^n$  from its degraded measurements  $y \in \mathbb{R}^m$  obtained with the degradation model:

$$(2.1) \quad y = Ax + \epsilon,$$

where  $A \in \mathbb{R}^{m \times n}$  represents the degradation operator depending on the inverse problem and  $\epsilon \in \mathbb{R}^m$  typically represents Additive White Gaussian Noise (AWGN). The restoration of these degraded images is an ill-posed problem, therefore a prior is used to restrict the set of solutions. The reconstruction can be treated using Bayesian estimation that uses the posterior conditional probability  $p(x|y)$ . Maximum a posteriori probability (MAP) is the most popular estimator in this scheme, where we choose  $x$  that maximizes  $p(x|y)$ . The estimation task is hence modeled as the optimization problem

$$(2.2) \quad \hat{x}_{MAP} = \operatorname{argmax}_x p(x|y) = \operatorname{argmax}_x \frac{p(y|x)p(x)}{p(y)},$$

$$(2.3) \quad = \operatorname{argmin}_x -\log(p(y|x)) - \log(p(x)),$$

where  $p(y|x)$  and  $p(x)$  are respectively the likelihood and the prior distributions. For the linear degradation model in [Equation 2.1](#) with Additive White Gaussian Noise  $\epsilon$  of standard deviation  $\sigma$ , we get

$$(2.4) \quad \hat{x}_{MAP} = \operatorname{argmin}_x \frac{1}{2} \|y - Ax\|_2^2 + \sigma^2 \phi(x),$$

where the data fidelity term  $f(x) = \frac{1}{2} \|y - Ax\|_2^2$  enforces the similarity with the degraded measurements, whereas the regularization term  $\phi(x)$  reflects prior knowledge and a property to be satisfied by the searched solution. The non-negative weighting parameter  $\sigma^2$  balances

the trade-off between the two terms. The problem in [Equation 2.4](#) does not have a closed-form solution in general. Therefore it must be solved using different optimization algorithms. The Plug-and-Play framework typically considers proximal splitting algorithms which decompose the problem in two sub-problems (one for each term in [Equation 2.4](#)) and solve them alternately. In these algorithms, the regularization sub-problem consists in evaluating the proximal operator of the regularization term defined as:

$$(2.5) \quad \begin{aligned} \text{prox}_{\sigma^2\phi}(z) &= \underset{x}{\operatorname{argmin}} \mathcal{F}_\phi(x, z, \sigma), \\ \text{with } \mathcal{F}_\phi(x, z, \sigma) &= \frac{1}{2} \|x - z\|_2^2 + \sigma^2 \phi(x). \end{aligned}$$

This can be seen as a particular case of inverse problem where the degradation operator  $A$  is the identity matrix, and the degradation only consists in the addition of White Gaussian Noise of standard deviation  $\sigma$ . The proximal operator in [Equation 2.5](#) can thus be interpreted as a MAP Gaussian denoiser. Hence, this sub-problem can be conveniently replaced by a state-of-the-art Gaussian denoiser in a Plug-and-Play proximal algorithm.

However, this approach does not directly generalize to the gradient descent algorithm where the update formula for the minimization in [Equation 2.4](#) is expressed as:

$$(2.6) \quad \hat{x}_{k+1} = \hat{x}_k - \mu \nabla \mathcal{F}_\phi(\hat{x}_k),$$

$$(2.7) \quad = \hat{x}_k - \mu \left[ \nabla f(\hat{x}_k) + \sigma^2 \cdot \nabla \phi(\hat{x}_k) \right],$$

$$(2.8) \quad = \hat{x}_k - \mu \left[ A^T (A\hat{x}_k - y) + \sigma^2 \cdot \nabla \phi(\hat{x}_k) \right].$$

Here, instead of the proximal operator of the regularizer  $\phi$ , we need its gradient  $\nabla \phi$ , which cannot be replaced by a denoiser. In this paper, we propose to train a network that can serve as the gradient of the regularization term in Plug-and-Play gradient descent algorithms.

### 3. Training of the gradient of a regularizer.

**3.1. Mathematical derivations.** We show in the following that it is mathematically possible to train a network that corresponds to the gradient of a regularizer by using a deep denoiser. Let us consider a denoiser  $\mathcal{D}_\sigma$  defined as the proximal operator in [Equation 2.5](#):

$$(3.1) \quad \mathcal{D}_\sigma(z) = \underset{x}{\operatorname{argmin}} \mathcal{F}_\phi(x, z, \sigma).$$

Hence, for  $\sigma$  and  $z$  fixed, the denoised image  $x = \mathcal{D}_\sigma(z)$  minimizes  $\mathcal{F}_\phi(x, z, \sigma)$ . Therefore, we have:

$$(3.2) \quad \left. \frac{\partial \mathcal{F}_\phi}{\partial x} \right|_{x=\mathcal{D}_\sigma(z)} = 0,$$

Furthermore,  $\frac{\partial \mathcal{F}_\phi}{\partial x}$  can be computed as:

$$(3.3) \quad \frac{\partial \mathcal{F}_\phi}{\partial x} = \frac{\partial \left[ \frac{1}{2} \|x - z\|_2^2 + \sigma^2 \phi(x) \right]}{\partial x},$$

$$(3.4) \quad = x - z + \sigma^2 \cdot \frac{\partial \phi(x)}{\partial x}.$$

Evaluating at the denoised image  $x = \mathcal{D}_\sigma(z)$  thus gives:

$$(3.5) \quad \left. \frac{\partial \mathcal{F}_\phi}{\partial x} \right|_{x=\mathcal{D}_\sigma(z)} = \mathcal{D}_\sigma(z) - z + \sigma^2 \cdot \left. \frac{\partial \phi(x)}{\partial x} \right|_{x=\mathcal{D}_\sigma(z)}.$$

Using Equation 3.2 and Equation 3.5, we obtain:

$$(3.6) \quad \mathcal{D}_\sigma(z) - z + \sigma^2 \cdot \left. \frac{\partial \phi(x)}{\partial x} \right|_{x=\mathcal{D}_\sigma(z)} = 0,$$

$$(3.7) \quad \sigma^2 \cdot \left. \frac{\partial \phi(x)}{\partial x} \right|_{x=\mathcal{D}_\sigma(z)} = z - \mathcal{D}_\sigma(z),$$

$$(3.8) \quad \sigma^2 \cdot \nabla \phi(\mathcal{D}_\sigma(z)) = z - \mathcal{D}_\sigma(z).$$

Using Equation 3.8, we can train a network that corresponds to the gradient of the regularizer  $\nabla \phi$  with respect to its input using the loss function

$$(3.9) \quad \mathcal{L}_{\nabla \phi} = \left\| \sigma^2 \cdot \nabla \phi(\mathcal{D}_\sigma(z)) - (z - \mathcal{D}_\sigma(z)) \right\|_2^2.$$

This requires the knowledge of the corresponding denoiser  $\mathcal{D}_\sigma$ . Note that Equation 3.8 is valid for any value of  $\sigma$  regardless of the degradation in  $z$ . Hence,  $\sigma$  can be seen as a free parameter of our loss  $\mathcal{L}_{\nabla \phi}$ . For small values of  $\sigma$ , the input  $\mathcal{D}_\sigma(z)$  of the regularizing network  $\nabla \phi$  will be close to the degraded image  $z$ . Hence  $\nabla \phi$  will be trained to fit the artifacts in the degraded images (e.g. noise). On the other hand, for high values of  $\sigma$ , the input of  $\nabla \phi$  will be a strongly denoised image, with reduced artifacts but less details. Hence,  $\nabla \phi$  will be trained to recover the missing details. During the training, we vary the value of this parameter so that the regularizing network can recover details while also removing artifacts (see details in Subsection 3.2).

Also note that in practice, since  $\phi$  is meant to be used in gradient-based algorithms, we only need the gradient  $\nabla \phi$  rather than an explicit definition of  $\phi$ . Hence, we propose in what follows a framework for end-to-end training of  $\nabla \phi$  along with the denoiser  $\mathcal{D}$ .

**3.2. Training framework for the regularizer's gradient.** The training framework is depicted in Figure 1. Let  $\eta \rightarrow \mathcal{N}(0, \sigma_0)$  be a white Gaussian noise of mean 0 and standard deviation  $\sigma_0$  that we use to corrupt the ground truth images  $x_0$  of the training dataset to produce degraded images  $z = x_0 + \eta$ . Let  $\sigma$  be a standard deviation value used as a parameter of our loss  $\mathcal{L}_{\nabla \phi}$ , as defined in Subsection 3.1. In order to handle different values of  $\sigma$  in Equation 3.9,  $\mathcal{D}_\sigma$  is modelled as a non-blind deep denoiser that takes as input a noise level map (i.e. each pixel of the noise level map being equal to  $\sigma$ ) concatenated with the noisy image  $z$ . For the denoiser, we use a simple  $l_1$  loss defined as:

$$(3.10) \quad \mathcal{L}_{D_\sigma} = \|\mathcal{D}_\sigma(z) - x_0\|_1.$$

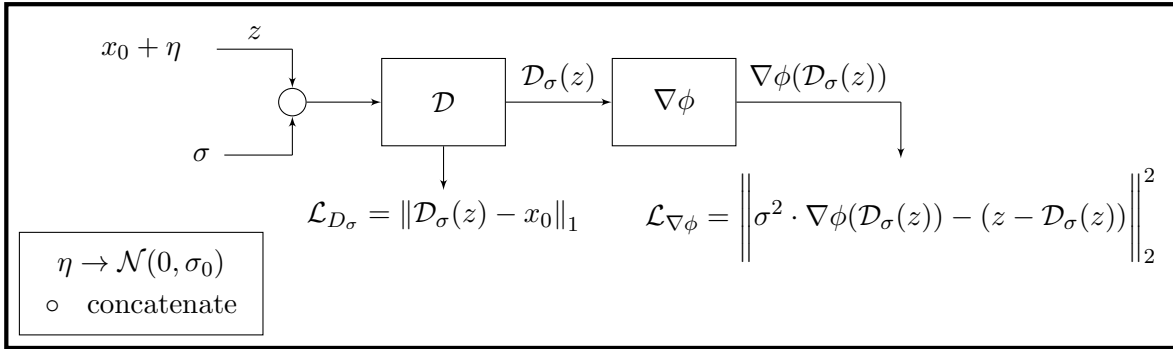


**Figure 1.** Framework for end-to-end training of  $\mathcal{D}$  and  $\nabla\phi$ .

Note that Equation 3.10 is a suitable loss for the denoiser only when  $\sigma = \sigma_0$  since the non-blind denoiser must be parameterized with the true noise level  $\sigma_0$  of the noisy input. The denoised output  $\mathcal{D}_\sigma(z)$  is then inputted to the network modelling the gradient of the regularizer in order to train it using the loss  $\mathcal{L}_{\nabla\phi}$  defined in Equation 3.9.

Hence, our goal is to minimize the global loss defined as:

$$(3.11) \quad \mathcal{L} = \delta \mathcal{L}_{\mathcal{D}_\sigma} + \lambda \mathcal{L}_{\nabla\phi},$$

$$\text{where } \lambda > 0 \text{ and } \delta = \begin{cases} 1 & \text{if } \sigma_0 = \sigma \\ 0 & \text{otherwise} \end{cases}.$$

For training the deep denoiser network, we should set the noise level  $\sigma$  inputted to the network equal to the actual noise level  $\sigma_0$  used for generating  $\eta$ . However, as explained in Subsection 3.1, for the loss  $\mathcal{L}_{\nabla\phi}$ , it is preferable to select  $\sigma$  independently of  $\sigma_0$ . Hence, the input  $\mathcal{D}_\sigma(z)$  of our regularizer gradient network  $\nabla\phi$  can cover a wide range of alterations, including images with remaining noise (i.e.  $\sigma < \sigma_0$ ) or with too strong denoising, and thus less details (i.e.  $\sigma > \sigma_0$ ). We therefore choose to alternate during the training between either selecting independently  $\sigma$  and  $\sigma_0$ , or setting  $\sigma = \sigma_0$  in order to keep  $\mathcal{D}$  faithful to the data. Furthermore, since the denoiser loss  $\mathcal{L}_{\mathcal{D}_\sigma}$  is only valid when  $\sigma = \sigma_0$ , we omit this loss when  $\sigma \neq \sigma_0$  by setting  $\delta = 0$ .

Note that an alternative training strategy would consist in first training the denoiser separately (only with the loss  $\mathcal{L}_{\mathcal{D}_\sigma}$ ), and then training the regularizer (only with the loss  $\mathcal{L}_{\nabla\phi}$ ) without jointly updating the denoiser. However, separately training the denoiser only ensures good denoising performance, but it does not guarantee to match the formal definition of a MAP Gaussian denoiser for some differentiable prior, i.e. a proximal operator of a differentiable scalar function  $\phi$ . We further analyse the advantages of jointly training the denoiser and the regularizer in Subsection 4.3.

**3.3. Training details.** For our training, we use a state-of-the-art deep denoiser architecture in order to train our network modelling the gradient of the regularizer. We choose to work with the DRUNet proposed in [46] which is a combination of U-Net [33] and ResNet [18]. Since it takes as input the noisy image concatenated in the channel dimension with a noise level map, it can suitably represent the non-blind denoiser  $\mathcal{D}_\sigma$ .

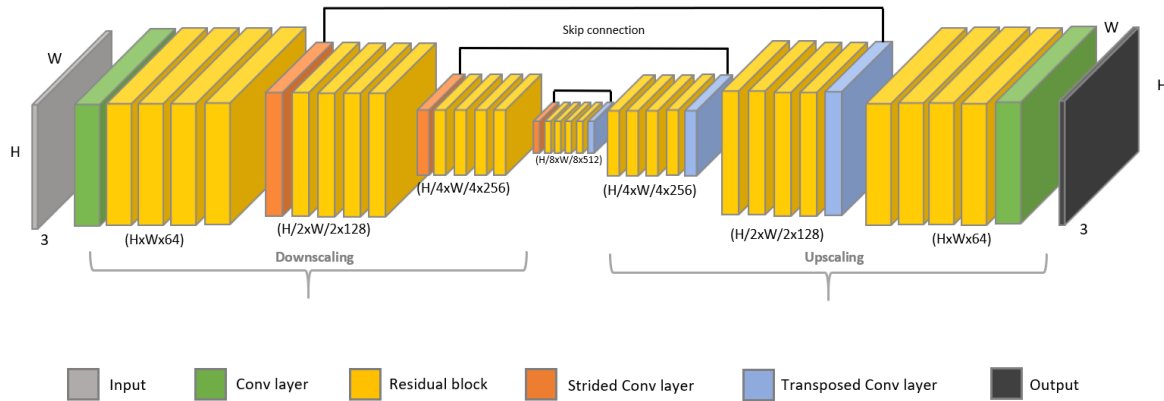


**Figure 2.** Architecture of the DRUNet network [46], that we choose for our  $\nabla\phi$  by changing the input channel to 3 instead of 4 (the regularizer doesn't need a noise level map as additional input).

The architecture of the regularizing network  $\nabla\phi$  is shown in Figure 2. It is the same architecture as the DRUNet denoiser, with the only difference that it does not take a noise level map as additional input.

We initialize  $\mathcal{D}_\sigma$  using the pre-trained DRUNet denoiser (which we reproduced based on the work in [46]). Then, we train our network  $\nabla\phi$  while jointly updating  $\mathcal{D}_\sigma$ , following the proposed framework in Subsection 3.2. The weight  $\lambda$  of the loss  $\mathcal{L}_{\nabla\phi}$  in Equation 3.11 is set equal to 0.004. The selection of the parameters  $\sigma$  and  $\sigma_0$  follows the alternating strategy described in Subsection 3.2: for half of the training iterations, we use  $\sigma = \sigma_0$  with a value chosen randomly with uniform distribution in  $[0, 50]$ ; otherwise,  $\sigma$  and  $\sigma_0$  are chosen independently with the same uniform distribution.

The remaining training details are similar to the ones presented in [46] for the DRUNet pre-training: the same large dataset of 8694 images composed of images from the Waterloo Exploration Database [26], the Berkeley Segmentation Database [7], the DIV2K dataset [1] and the Flick2K dataset [24] is used. 16 patches of 128x128 are randomly sampled from the training dataset for each iteration. We use the ADAM optimizer [20] to minimize the loss  $\mathcal{L}$  defined in Equation 3.11. The learning rate is initially set to 1e-4, and decreased by half every 100,000 iterations until reaching 5e-7, where the training stops.

## 4. Experimental results.

**4.1.  $\nabla\phi$  for Plug-and-Play gradient descent.** In this section, we evaluate the performance of our approach. First, we propose to use our network to solve different inverse problems in a simple Plug-and-Play gradient descent algorithm. For experimental results, we use the ADAM optimizer to solve Equation 2.4 with the Plug-and-Play gradient descent.

As the main goal of this approach is to solve inverse problems using simple gradient-based algorithms with a generic regularizer, we compare ourselves to algorithms that are designed to solve different inverse problems using a single regularization network in a Plug-and-Play framework. Hence, we compare the performance of our network to the PnP-ADMM with the



DRUNet [46], the RED [32] in gradient descent with the DRUNet used for regularization, and Chang’s projection operator [31] used in an ADMM framework. We also compare with the Deep Image Prior (DIP) [40], which is a generative model trained for each test image in an unsupervised way. The network takes a random input vector and adjusts its weights to minimize the mean square error (MSE) between its output after applying the degradation and the true degraded observation. This method can be seen as a generic approach as well.

For fair comparisons, we reproduced all the results under the same conditions, i.e. using the same initialization and the same degradation operator  $A$  for each application as described in the following subsections. To reproduce the results of [31] we used the model trained by the authors, which takes input images of size 64x64. Hence we applied the network on quarter-overlapping sample patches in order to enhance the results by avoiding block artifacts.

We tuned the parameters of each of these methods for each application in order to get the best results. Table 1 shows the parameters used during testing for the Plug-and-Play gradient descent with our regularizer. In theory, the parameter  $\sigma$  in Equation 2.4 should be equal to the true standard deviation  $\sigma_n$  of the Gaussian noise added on the degraded image. However, when  $\sigma_n = 0$  (e.g. super-resolution, pixel-wise inpainting), choosing  $\sigma = 0$  would completely remove the regularization term. For these cases, we choose a small non-zero value of  $\sigma$  depending on the application.

**Table 1**

*Parameters used for the Plug-and-Play gradient descent with our regularizer.  $\mu$ : gradient step size,  $\sigma$ : weight of the regularization,  $\sigma_n$ : standard deviation of the AWGN added on the degraded image*

		$\sigma_n$	$\mu$	$\sigma$
Super-Resolution x2	Bicubic	0	0.008	1.2/255
	Gaussian	0	0.008	0.8/255
Super-Resolution x3	Bicubic	0	0.002	0.9/255
	Gaussian	0	0.004	0.4/255
Deblurring	$\sigma_b = 1.6$	$\sqrt{2}/255$	0.005	$\sqrt{2}/255$
	$\sigma_b = 2.0$	$\sqrt{2}/255$	0.005	$\sqrt{2}/255$
Pixel-wise inpainting	0.1	0	0.01	1/255
	0.2	0	0.025	3.6/255

#### 4.1.1. Super-Resolution.

Super-resolution consists of reconstructing a high-resolution image from a low-resolution (i.e. downsampled) measurement. Low resolution images are generated by applying a convolution kernel followed by a downsampling by a factor  $t$ . We evaluate our method with bicubic and Gaussian convolutional kernels, with both 2x and 3x downsampling scales. The Gaussian kernel has a standard deviation  $\sigma_b = 0.5 \cdot t$  (i.e.  $\sigma_b = 1$  for x2 and  $\sigma_b = 1.5$  for x3). In all the cases, the gradient descent is initialized with a high resolution image obtained by bicubic upsampling of the degraded image.

Tables 2 and 3 show a numerical comparison of our method with the aforementioned generic approaches for super-resolution of factor 2 and 3 respectively, for both bicubic and



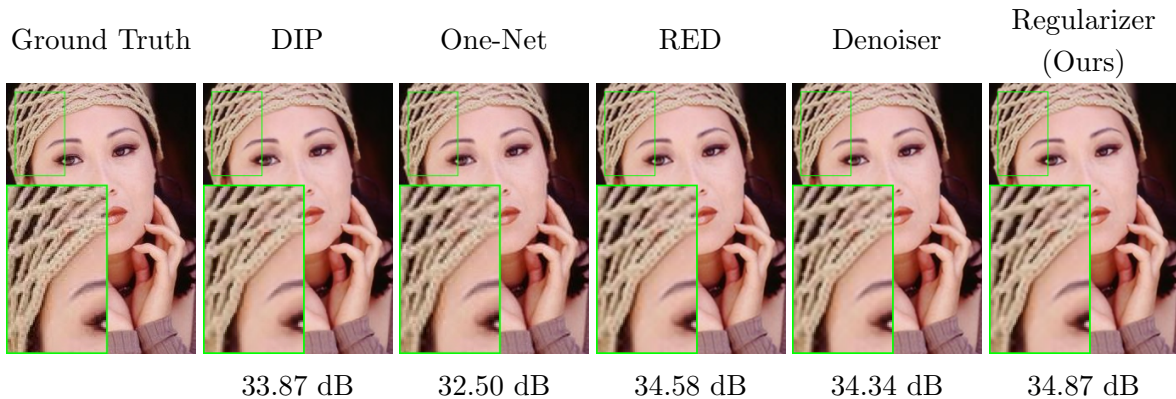


**Figure 3.** Visual comparison of super-resolution results obtained with the DIP [40], the projection operator (One-Net) [31], RED [32], PnP-ADMM [46] and our regularizer used in a PnP-GD framework. Low resolution images generated with a bicubic kernel followed by a downsampling by a factor of 2.

Gaussian filters. A bicubic interpolation of the degraded image was used for initialization. The PSNR (peak signal-to-noise ratio) measures presented in this paper are computed on the RGB channels. Numerical comparison gives higher values for the regularizer compared to the existing generic Plug-and-Play approaches, with a slight improvement with respect to the PnP-ADMM. Figure 3 shows a visual comparison of the results for a degradation with a bicubic kernel and a downsampling by a factor of 2. We observe sharper images with less aliasing artifacts produced by our approach.

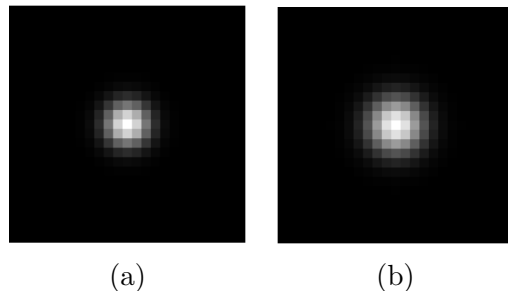


**Figure 4.** Blurring Gaussian kernels of standard deviation of (a) 1.6 and (b) 2.0

#### 4.1.2. Deblurring.

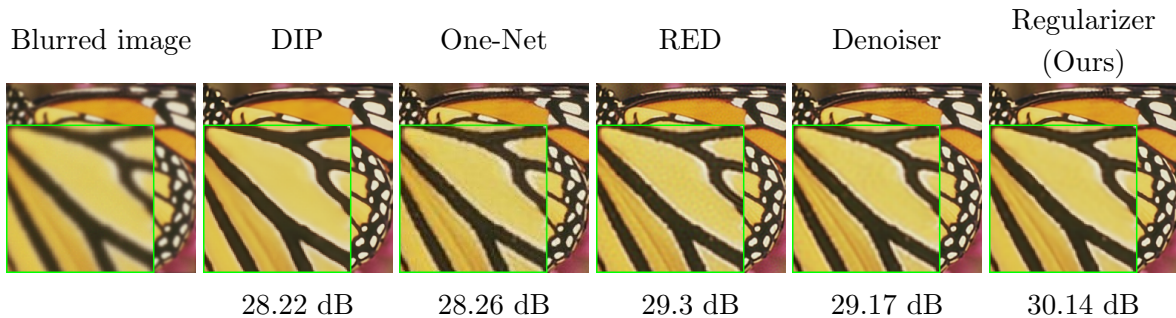
For image deblurring, the degradation consists of a convolution performed with circular boundary conditions. Hence, the degradation matrix can be written as  $A = \mathcal{F}^* D \mathcal{F}$ , where  $\mathcal{F}$  and  $\mathcal{F}^*$  represent respectively the discrete Fourier transform and its inverse, and  $D$  is a diagonal matrix representing the filter in the Fourier domain. We degrade our images with two 25x25 isotropic Gaussian blur kernels of standard deviations of 1.6 and 2.0 (Figure 4) that are used in [45], and add a White Gaussian noise of standard deviation  $\sigma_n = \sqrt{2}/255$ . The blurred image is directly used as the initialization of the Plug-and-Play gradient descent.

Table 4 shows the PSNR results [dB] of the evaluation of our method for deblurring.

**Table 2**

Super-resolution results obtained with our regularizer used in Plug-and-Play gradient descent (corrupted with bicubic and Gaussian kernels and downsampled by a factor of 2), measured in terms of PSNR [dB]. Comparison with DIP [40], the projection operator (One-Net) [31], RED [32] and the PnP-ADMM [46].

		DIP	One-Net	RED	PnP-ADMM	Ours
(i) Bicubic	Baby	35.49	36.87	37.31	37.33	<b>37.43</b>
	Bird	37.85	36.88	39.69	<b>40.29</b>	40.08
	Butterfly	31.43	27.78	31.57	31.87	<b>32.24</b>
	Head	31.65	32.06	32.10	<b>32.26</b>	32.13
	Women	33.87	32.50	34.58	34.34	<b>34.87</b>
	Average	34.06	33.22	35.05	35.22	<b>35.35</b>
(i) Gauss	Baby	35.21	36.43	37.26	37.27	<b>37.35</b>
	Bird	37.36	36.15	39.54	<b>40.18</b>	39.97
	Butterfly	30.98	27.13	31.52	31.83	<b>32.18</b>
	Head	31.48	31.80	32.09	<b>32.23</b>	32.07
	Women	33.52	31.80	34.54	34.27	<b>34.82</b>
	Average	33.71	32.67	34.99	35.16	<b>35.28</b>



**Figure 5.** Visual comparison of deblurring results obtained with the DIP [40], the projection operator (One-Net) [31], RED [32], PnP-ADMM [46] and our regularizer used in a PnP-GD framework. The blurred images are generated by an isotropic Gaussian kernel of standard deviation 1.6.

Similarly to super-resolution, we observe higher PSNR values with respect to the other generic methods for both Gaussian kernels of standard deviation 1.6 and 2.0. Visual comparison in Figure 5 shows that our approach successfully recovers the details without increasing the noise.

#### 4.1.3. Pixel-wise inpainting.

Pixel-wise inpainting consists of restoring pixel-values in an image where a number of the pixels were randomly dropped. The degradation consists of multiplying the ground-truth image by a binary mask. For the initialization image  $\hat{x}^0$ , we set the color of the unknown pixels to grey. We test our results with both 20% and 10% of known pixels rates.

Table 5 shows a numerical evaluation of our method for the application of pixel-wise inpainting in terms of PSNR [dB]. We observe significant performance gains of our regularizer compared to the other methods, especially in the most challenging case where the known pixel

Table 3

Super-resolution results obtained with our regularizer used in Plug-and-Play gradient descent (corrupted with bicubic and Gaussian kernels and downsampled by a factor of 3), measured in terms of PSNR [dB]. Comparison with DIP [40], the projection operator (One-Net) [31], RED [32] and the PnP-ADMM [46].

		DIP	One-Net	RED	PnP-ADMM	Ours
(i) Bicubic	Baby	33.47	33.45	34.10	34.06	<b>34.14</b>
	Bird	34.06	31.95	34.45	<b>34.99</b>	34.80
	Butterfly	27.93	23.95	27.22	27.43	<b>27.56</b>
	Head	30.55	30.41	<b>30.81</b>	30.77	<b>30.81</b>
	Women	30.55	28.47	<b>30.80</b>	30.45	30.62
	Average	31.31	29.65	31.47	31.54	<b>31.59</b>
(i) Gauss	Baby	32.98	33.32	34.07	34.00	<b>34.12</b>
	Bird	33.69	31.73	34.39	<b>34.90</b>	34.74
	Butterfly	27.79	23.93	27.19	27.43	<b>27.56</b>
	Head	30.49	30.27	30.78	30.73	<b>30.82</b>
	Women	30.45	28.37	<b>30.77</b>	30.40	30.35
	Average	31.08	29.52	31.44	31.49	<b>31.52</b>

Table 4

Deblurring results obtained with our regularizer used in Plug-and-Play gradient descent (blurred images are generated by isotropic Gaussian kernels of standard deviation 1.6 and 2.0), measured in terms of PSNR [dB]. Comparison with DIP [40], the projection operator (One-Net) [31], RED [32] and the PnP-ADMM [46].

		DIP	One-Net	RED	PnP-ADMM	Ours
(i) $\sigma = 1.6$	Baby	32.55	34.71	34.54	34.94	<b>35.43</b>
	Bird	33.63	34.69	35.57	36.52	<b>36.90</b>
	Butterfly	28.22	28.26	29.3	29.17	<b>30.14</b>
	Head	30.24	31.14	30.96	31.12	<b>31.24</b>
	Women	30.84	32.07	32.16	32.41	<b>32.91</b>
	Average	31.1	32.18	32.51	32.83	<b>33.32</b>
(i) $\sigma = 2.0$	Baby	31.76	33.76	33.71	33.86	<b>34.22</b>
	Bird	32.14	32.81	34.3	34.63	<b>35.01</b>
	Butterfly	26.86	25.48	27.51	27.61	<b>28.19</b>
	Head	29.7	30.29	30.58	30.63	<b>30.69</b>
	Women	29.15	29.70	30.89	31.01	<b>31.26</b>
	Average	29.92	30.41	31.40	31.55	<b>31.87</b>

rate is only 10%. The visual improvements can also be seen in Figure 6.

**4.2. Unrolled gradient descent with  $\nabla\phi$ .** Aside from the Plug-and-Play gradient descent, our approach for training  $\nabla\phi$  can also serve as a pre-training strategy for unrolled gradient descent. In unrolled optimization methods, the regularization network is trained for each inverse problem such that applying a fixed number of iterations of the algorithm (e.g. Equation 2.6 for gradient descent) best approximates the ground truth image. We describe the unrolled

Table 5

Pixel-wise inpainting results obtained with our regularizer used in Plug-and-Play gradient descent (Corrupted images are generated by keeping 20% and 10% of the known pixels), measured in terms of PSNR [dB]. Comparison with DIP [40], the projection operator (One-Net) [31], RED [32] and the PnP-ADMM [46].

		DIP	One-Net	RED	PnP-ADMM	Ours
(i) 0.2	Baby	31.72	28.64	29.05	33.04	<b>33.08</b>
	Bird	32.85	26.92	27.74	<b>33.96</b>	33.95
	Butterfly	24.91	20.65	23.51	24.99	<b>25.51</b>
	Head	29.07	25.06	28.11	29.60	<b>29.82</b>
	Women	28.64	19.05	27.41	29.41	<b>29.45</b>
	Average	29.44	24.06	27.17	30.20	<b>30.36</b>
(i) 0.1	Baby	29.76	18.71	26.35	<b>30.26</b>	30.20
	Bird	29.15	18.42	23.11	28.78	<b>29.34</b>
	Butterfly	<b>21.56</b>	13.93	16.35	20.34	21.06
	Head	27.82	21.17	26.11	27.92	<b>28.07</b>
	Women	25.84	13.76	21.85	23.73	<b>26.03</b>
	Average	26.83	17.20	22.75	26.2	<b>26.94</b>



Figure 6. Visual comparison of pixel-wise inpainting results with known pixel rate of  $p = 20\%$ , obtained with the DIP [40], the projection operator (One-Net) [31], RED [32], PnP-ADMM [46] and our regularizer used in a PnP-GD framework.

training approach in Algorithm 4.1 for a gradient descent optimization. While this end-to-end training strategy loses the genericity of the Plug-and-Play approach, it typically improves the performances.

However, to facilitate the training, it is generally required to initialize the network weights with a generically pre-trained version. When unrolling proximal algorithms such as ADMM, a pre-trained deep denoiser can be used since it can be interpreted as the proximal operator of a generic regularization function. On the other hand, the gradient descent requires instead the gradient of a regularizer. Hence, a denoiser cannot be directly used as a pre-trained network. By transferring the image prior implicitly represented by the denoiser to our regularizer's gradient  $\nabla\phi$ , our method thus provides a satisfying pre-trained network for unrolled gradient descent.

We tested this approach for super-resolution of factor 2 and 3, as well as deblurring with 2

Table 6

Parameters used for unrolled gradient descent optimization for both pre-trained and not pre-trained versions (i) Super-Resolution of factor 2 and 3 for bicubic corruption (ii) Deblurring with an isotropic Gaussian kernel of standard deviation of 1.6 and 2.0 .  $\sigma_n$ : Standard deviation of the White Gaussian noise added on the corrupted image,  $\sigma$ : weight of the regularization term,  $\mu$ : gradient step size ,  $N$ : number of unrolled iterations. The training is performed over the DIV2K dataset [1].

	(i) Super-Resolution		(ii) Deblurring	
	x2	x3	$\sigma_b = 1.6$	$\sigma_b = 2.0$
$\sigma_n$	0	0	$\sqrt{2}/255$	$\sqrt{2}/255$
$\sigma$	1.2/255	1.6/255	$\sqrt{2}/255$	$\sqrt{2}/255$
$\mu$	0.008	0.1	0.004	0.004
$N$	6	6	6	6

---

**Algorithm 4.1** Unrolled gradient descent with  $\nabla\phi$ 


---

```

1: initialize  $\nabla\phi, \sigma_n, \mu, A, B$ 
2: for each epoch do
3:   for each batch do
4:      $\eta \leftarrow \mathcal{N}(0, \sigma_n)$ 
5:      $x_{gt} \leftarrow$  ground-truth batch
6:      $y \leftarrow Ax_{gt} + \eta$ 
7:      $x_0 \leftarrow y$ 
8:     for  $k \leftarrow 0$  to  $N - 1$  do
9:        $x_{k+1} \leftarrow x_k - \mu[A^T(Ax_k - y) + \sigma^2\nabla\phi(x_k)]$ 
10:    end for
11:    loss  $\leftarrow \|x_N - x_{gt}\|_2^2$ 
12:    Update weights of  $\nabla\phi$  with back-propagation
13:  end for
14: end for

```

---

isotropic Gaussian kernels (with standard deviations of 1.6 and 2.0) and compared our results with a network learned end-to-end in an unrolled environment without the pre-training (i.e. random weight initialization).

Both versions (pre-trained and not pre-trained) were unrolled in the same conditions. Table 6 shows the training parameters for each of the different tasks. For all 4 cases, we trained over the DIV2K dataset [1] of 800 images, over 600 epochs by randomly taking 48x48 patches from the dataset. In addition, we include a comparison with the Total Deep Variation (TDV) method [21] which also performs unrolled optimisation where the network represents the gradient of the regularization function. In [21], the network is not pre-trained. Instead, the training starts with a small number of unrolled iterations  $N = 2$ , and  $N$  is incremented every 700 epochs. Note that the authors originally trained the TDV network for  $N = 10$  iterations of an unrolled proximal gradient descent algorithm. However, for fair comparisons



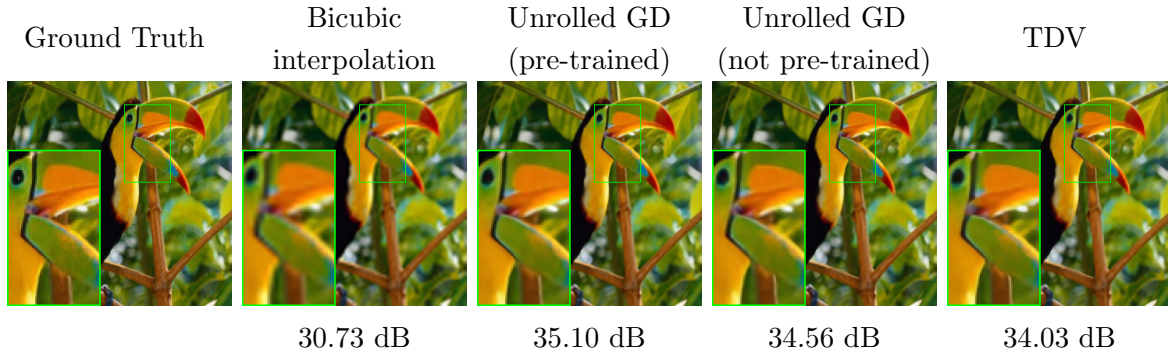


**Figure 7.** Visual comparison of super-resolution results between unrolled gradient descent with and without pre-training. Low resolution images generated with a bicubic kernel followed by a downsampling by a factor of 3.

with our approach, we re-trained it with  $N = 6$  iterations of simple unrolled gradient descent.

Tables 7 and 8 show the PSNR results [dB] for both networks (pre-trained and not pre-trained) as well as the TDV for super-resolution and deblurring respectively, on Set5, Set14 and BSDS100. As expected, using  $\nabla\phi$  for weight initialization improves the results of the unrolled gradient descent for all of the 4 tested cases (with up to 0.9 dB). Some visual comparisons of super-resolution with magnifying factor of 3 and deblurring images corrupted by a Gaussian kernel of standard deviation 2.0 are respectively shown in Figures 7 and 8. The visual results confirm that better reconstruction of the details is obtained when our pre-training is used. While the TDV results display even sharper edges, the PSNR remains lower because of exaggerated sharpness in comparison to the ground truth.

**Table 7**

Super-resolution results obtained with unrolled gradient descent (corrupted with bicubic kernel and down-sampled by a factor of 2 and 3), measured in terms of PSNR [dB] and evaluated on Set5, Set14 and BSDS100. Restoration obtained with unrolled gradient descent initialized with our pre-trained network  $\nabla\phi$  and without weight initialization, as well as TDV [21]

		pre-trained (ours)	not pre-trained	TDV
(i) x2	Set5	35.61	35.42	34.57
	Set14	31.18	30.93	30.31
	BSDS100	30.77	30.68	30.23
(i) x3	Set5	32.1	31.88	31.47
	Set14	28.00	27.79	27.40
	BSDS100	27.68	27.63	27.34

**4.3. Analysis of the joint training.** In this section, we verify experimentally the advantages of updating the denoising network within the training of our network  $\nabla\phi$ , compared to letting the denoiser fixed. In the latter case,  $\delta$  is always set to 0 (i.e.  $\mathcal{L} = \lambda\mathcal{L}_{\nabla\phi}$ ).

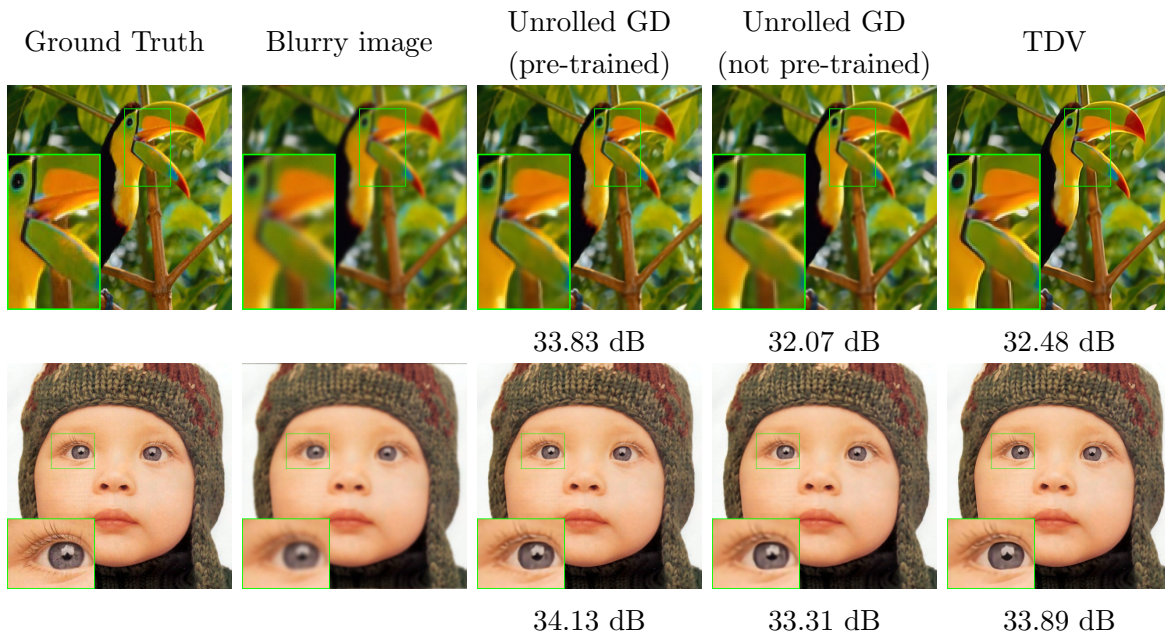


**Figure 8.** Visual comparison of deblurring results between unrolled gradient descent with and without pre-training. The blurred images are generated by an isotropic Gaussian kernel of standard deviation 2.0.

**Table 8**

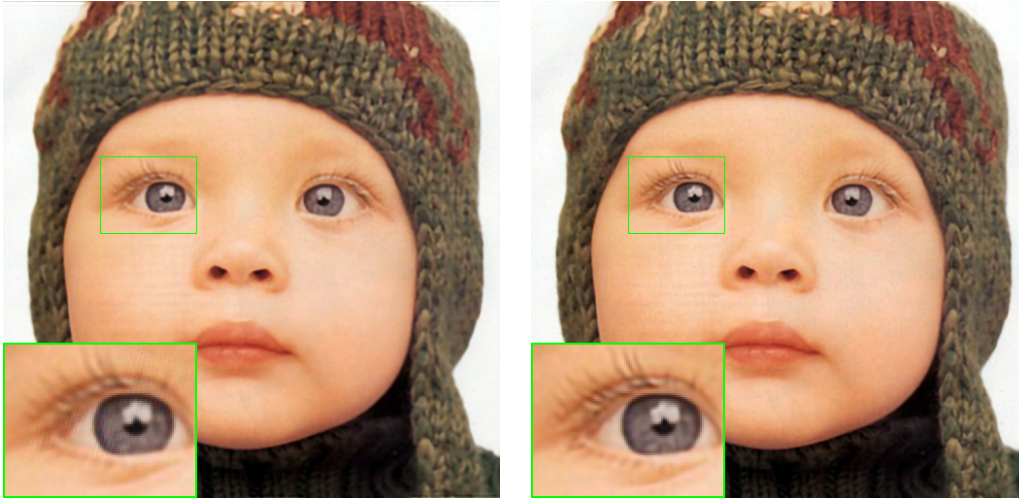
Deblurring results obtained with unrolled gradient descent (corrupted with isotropic Gaussian kernels with standard deviation 1.6 and 2.0), measured in terms of PSNR [dB] and evaluated on Set5, Set14 and BSDS100. Restoration obtained with unrolled gradient descent initialized with our pre-trained network  $\nabla\phi$  and without weight initialization, as well as [21]

		pre-trained (ours)	not pre-trained	TDV
(i) $\sigma_0 = 1.6$	Set5	33.51	32.57	32.32
	Set14	30.14	29.33	29.17
	BSDS100	29.80	29.12	29.01
(ii) $\sigma_0 = 2$	Set5	31.63	30.94	30.52
	Set14	28.29	27.70	27.46
	BSDS100	28.08	27.52	27.51

First, we compare the performance of our regularizer’s gradient network trained in both scenarios. An example of deblurring results with the Plug-and-Play gradient descent is shown in Figure 9. It is clear that leaving the denoiser fixed to its pre-trained state degrades the performance of our network  $\nabla\phi$ : the reconstructed image in Figure 9 (a) remains more blurry than in Figure 9 (b) and it also presents colored fringes artifacts. On the other hand, when the denoiser is updated when training  $\nabla\phi$ , the convergence of the Plug-and-Play gradient descent

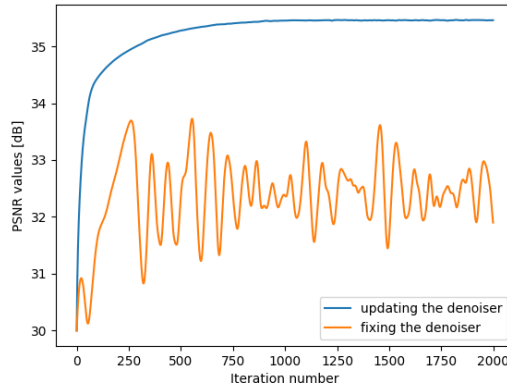


is significantly improved as well as the visual result, as shown in Figure 9 (b,c).



(a) 33.72 dB

(b) 35.46 dB



(c)

**Figure 9.** Comparison of the performances of the regularizer trained (a) along with a fixed denoiser and (b) when the denoiser weights are updated. (c) PSNR values along the PnP-GD iterations. Results of applying the regularizers in PnP-GD for deblurring (blurred images are generated by isotropic Gaussian kernels of standard deviation 1.6).

A possible explanation of the worse results when fixing the denoiser in our training is that the pre-training of  $\mathcal{D}_\sigma$  does not guarantee that there exists a differentiable regularizer  $\phi$  for which  $\text{prox}_{\sigma^2\phi} = \mathcal{D}_\sigma$  for every value of  $\sigma$ . In other words, the assumption that  $\mathcal{D}_\sigma$  is a MAP Gaussian denoiser for a differentiable prior may not be satisfied. However by jointly updating the denoiser with our network representing  $\nabla\phi$ , the modified denoiser better represents such a MAP Gaussian denoiser for the corresponding regularizer.

In a second experiment, we compare the performances of the updated denoiser and the original DRUNet when used in the Plug-and-Play ADMM algorithm. Figure 10 shows for each

ADMM iteration the PSNR of the reconstructed images and the MSE of the difference between two consecutive iterations for both versions of the denoiser. We can observe that although the original DRUNet can obtain better PSNR performances when stopping the ADMM after a few iterations (see subfigure (a)), the algorithm does not converge, and may even strongly diverge after a sufficiently large number of iterations. On the other hand our modified denoiser allows for a quick convergence of the Plug-and-Play ADMM.

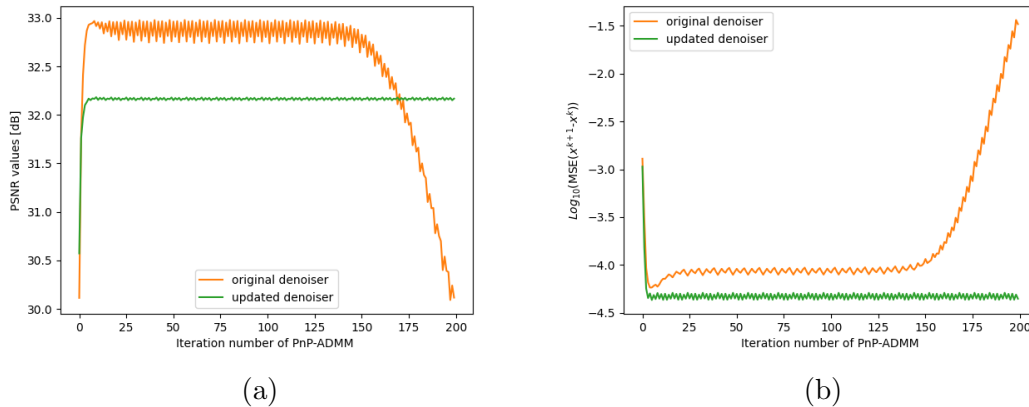


**Figure 10.** Comparison of the performances of the original and the updated denoisers in PnP-ADMM for deblurring on Set5 (The blurred images are generated by an isotropic Gaussian kernel of standard deviation 1.6): (a) Average PSNR over the ADMM iterations (b) MSE of the difference between two consecutive iterations (in log scale).

**5. Conclusion.** In this paper, we have proposed a novel framework for solving linear inverse problems. Our approach makes it possible to solve Plug-and-Play algorithms using gradient descent, where the gradient of the regularizer is required rather than its proximal operator. We have proved that it is mathematically possible to train a network that represents the gradient of a regularizer, jointly with a denoising neural network.

The results have demonstrated that the joint training of a regularizer’s gradient network with the DRUNet have several advantages. First, the regularizing network can be used in a Plug-and-Play gradient descent algorithm and outperform the performance of other generic approaches in different inverse problems such as super-resolution, deblurring and pixel-wise inpainting. Second, our network can also serve as a pre-training strategy for unrolled gradient descent and yield a significant improvement. Lastly, the joint training of the denoiser with the regularizing network makes the former match better the definition of a proximal operator compared to the original pre-trained DRUNet.

## REFERENCES

- [1] E. AGUSTSSON AND R. TIMOFTE, *Ntire 2017 challenge on single image super-resolution: Dataset and study*, in Proceedings of the IEEE conference on computer vision and pattern recognition workshops, 2017, pp. 126–135, <https://doi.org/10.1109/CVPRW.2017.150>.

- [2] S. BOYD, N. PARIKH, AND E. CHU, *Distributed optimization and statistical learning via the alternating direction method of multipliers*, Now Publishers Inc, 2011, <https://doi.org/10.1561/2200000016>.
- [3] A. BUADES, B. COLL, AND J.-M. MOREL, *A non-local algorithm for image denoising*, in *Computer Vision and Pattern Recognition*, vol. 2, 2005, pp. 60–65 vol. 2, <https://doi.org/10.1109/cvpr.2005.38>.
- [4] P. CASCARANO, A. SEBASTIANI, M. C. COMES, G. FRANCHINI, AND F. PORTA, *Combining weighted total variation and deep image prior for natural and medical image restoration via admm*, arXiv preprint arXiv:2009.11380, (2021), <https://doi.org/10.1109/ICCSA54496.2021.00016>.
- [5] A. CHAMBOLLE, V. CASELLES, D. CREMERS, M. NOVAGA, AND T. POCK, *An introduction to total variation for image analysis*, in *Theoretical foundations and numerical methods for sparse recovery*, de Gruyter, 2010, pp. 263–340, <https://doi.org/10.1515/9783110226157>.
- [6] S. H. CHAN, X. WANG, AND O. A. ELGENDY, *Plug-and-play admm for image restoration: Fixed-point convergence and applications*, *IEEE Transactions on Computational Imaging*, 3 (2016), pp. 84–98, <https://doi.org/10.1109/TCI.2016.2629286>.
- [7] Y. CHEN AND T. POCK, *Trainable nonlinear reaction diffusion: A flexible framework for fast and effective image restoration*, *IEEE transactions on pattern analysis and machine intelligence*, 39 (2016), pp. 1256–1272, <https://doi.org/10.1109/TPAMI.2016.2596743>.
- [8] K. DABOV, A. FOI, V. KATKOVNIK, AND K. EGIAZARIAN, *Image denoising by sparse 3-d transform-domain collaborative filtering*, *IEEE Transactions on image processing*, 16 (2007), pp. 2080–2095, <https://doi.org/10.1109/TIP.2007.901238>.
- [9] S. DIAMOND, V. SITZMANN, F. HEIDE, AND G. WETZSTEIN, *Unrolled optimization with deep priors*, arXiv preprint arXiv:1705.08041, (2017), <https://doi.org/10.48550/ARXIV.1705.08041>.
- [10] C. DONG, C. C. LOY, K. HE, AND X. TANG, *Learning a deep convolutional network for image super-resolution*, in *European conf. on computer vision*, Springer, 2014, pp. 184–199, [https://doi.org/10.1007/978-3-319-10593-2\\_13](https://doi.org/10.1007/978-3-319-10593-2_13).
- [11] J. DONG, S. ROTH, AND B. SCHIELE, *Deep wiener deconvolution: Wiener meets deep learning for image deblurring*, in *Advances in Neural Information Processing Systems*, H. Larochelle, M. Ranzato, R. Hadsell, M. Balcan, and H. Lin, eds., vol. 33, Curran Associates, Inc., 2020, pp. 1048–1059, <https://proceedings.neurips.cc/paper/2020/file/0b8aff0438617c055eb55f0ba5d226fa-Paper.pdf>.
- [12] T. EBOLI, J. SUN, AND J. PONCE, *End-to-end interpretable learning of non-blind image deblurring*, in *European Conference on Computer Vision*, Springer, 2020, pp. 314–331, [https://doi.org/10.1007/978-3-030-58520-4\\_19](https://doi.org/10.1007/978-3-030-58520-4_19).
- [13] M. A. FIGUEIREDO AND R. D. NOWAK, *An em algorithm for wavelet-based image restoration*, *IEEE Transactions on Image Processing*, 12 (2003), pp. 906–916, <https://doi.org/10.1109/TIP.2003.814255>.
- [14] D. GILTON, G. ONGIE, AND R. WILLETT, *Neumann networks for linear inverse problems in imaging*, *IEEE Transactions on Computational Imaging*, 6 (2019), pp. 328–343, <https://doi.org/10.1109/TCI.2019.2948732>.
- [15] K. GREGOR AND Y. LECUN, *Learning fast approximations of sparse coding*, in *Proceedings of the 27th international conference on international conference on machine learning*, 2010, pp. 399–406, <https://dl.acm.org/doi/10.5555/3104322.3104374>.
- [16] S. GU, Q. XIE, D. MENG, W. ZUO, X. FENG, AND L. ZHANG, *Weighted nuclear norm minimization and its applications to low level vision*, *International journal of computer vision*, 121 (2017), pp. 183–208, <https://doi.org/10.1007/s11263-016-0930-5>.
- [17] S. GU, L. ZHANG, W. ZUO, AND X. FENG, *Weighted nuclear norm minimization with application to image denoising*, in *Proceedings of the IEEE conference on computer vision and pattern recognition*, 2014, pp. 2862–2869, <https://doi.org/10.1109/CVPR.2014.366>.
- [18] K. HE, X. ZHANG, S. REN, AND J. SUN, *Deep residual learning for image recognition*, in *Proceedings of the IEEE conference on computer vision and pattern recognition*, 2016, pp. 770–778, <https://doi.org/10.1109/cvpr.2016.90>.
- [19] B. HENZ, E. S. GASTAL, AND M. M. OLIVEIRA, *Deep joint design of color filter arrays and demosaicing*, in *Computer Graphics Forum*, vol. 37, Wiley Online Library, 2018, pp. 389–399, <https://doi.org/10.1111/cgf.13370>.
- [20] D. P. KINGMA AND J. BA, *Adam: A method for stochastic optimization*, arXiv preprint arXiv:1412.6980, (2014), <https://doi.org/10.48550/arXiv.1412.6980>.
- [21] E. KOBLER, A. EFFLAND, K. KUNISCH, AND T. POCK, *Total deep variation for linear inverse problems*,

- in Conference on Computer Vision and Pattern Recognition (CVPR), Jun. 2020, pp. 7546–7555, <https://doi.org/10.1109/cvpr42600.2020.00757>.
- [22] C. LEDIG, L. THEIS, F. HUSZAR, J. CABALLERO, A. CUNNINGHAM, A. ACOSTA, A. P. AITKEN, A. TEJANI, J. TOTZ, AND Z. WANG, *Photo-realistic single image super-resolution using a generative adversarial network*, in IEEE Conf. on Computer Vision and Pattern Recognition (CVPR), 2017, p. 4681–4690, <https://doi.org/10.1109/cvpr.2017.19>.
- [23] S. LEFKIMMIATIS, J. P. WARD, AND M. UNSER, *Hessian Schatten-norm regularization for linear inverse problems*, IEEE transactions on image processing, 22 (2013), pp. 1873–1888, <https://doi.org/10.1109/TIP.2013.2237919>.
- [24] B. LIM, S. SON, H. KIM, S. NAH, AND K. MU LEE, *Enhanced deep residual networks for single image super-resolution*, in Proceedings of the IEEE conference on computer vision and pattern recognition workshops, 2017, pp. 136–144, <https://doi.org/10.1109/CVPRW.2017.151>.
- [25] J. LIU, Y. SUN, X. XU, AND U. S. KAMILOV, *Image restoration using total variation regularized deep image prior*, IEEE Int. Conf. on Acoustics, Speech and Signal Processing (ICASSP) pages = 7715–7719, (2019), <https://doi.org/10.1109/ICASSP.2019.8682856>.
- [26] K. MA, Z. DUANMU, Q. WU, Z. WANG, H. YONG, H. LI, AND L. ZHANG, *Waterloo exploration database: New challenges for image quality assessment models*, IEEE Transactions on Image Processing, 26 (2016), pp. 1004–1016, <https://doi.org/10.1109/TIP.2016.2631888>.
- [27] M. MARDANI, Q. SUN, S. VASAWANALA, V. POPYAN, H. MONAJEMI, J. PAULY, AND D. DONOHO, *Neural proximal gradient descent for compressive imaging*, arXiv preprint arXiv:1806.03963, (2018), <https://doi.org/10.48550/ARXIV.1806.03963>.
- [28] A. MOUSAVI AND R. G. BARANIUK, *Learning to invert: Signal recovery via deep convolutional networks*, in IEEE int. conf. on acoustics, speech and signal processing (ICASSP), IEEE, 2017, pp. 2272–2276, <https://doi.org/10.1109/ICASSP.2017.7952561>.
- [29] Q. NING, W. DONG, G. SHI, L. LI, AND X. LI, *Accurate and lightweight image super-resolution with model-guided deep unfolding network*, IEEE Journal of Selected Topics in Signal Processing, (2020), <https://doi.org/10.1109/JSTSP.2020.3037516>.
- [30] E. T. REEHORST AND P. SCHNITER, *Regularization by denoising: Clarifications and new interpretations*, IEEE transactions on computational imaging, 5 (2018), pp. 52–67, <https://doi.org/10.1109/TCI.2018.2880326>.
- [31] J. RICK CHANG, C.-L. LI, B. POCZOS, B. VIJAYA KUMAR, AND A. C. SANKARANARAYANAN, *One network to solve them all—solving linear inverse problems using deep projection models*, in Proceedings of the IEEE International Conference on Computer Vision, 2017, pp. 5888–5897, <https://doi.org/10.1109/iccv.2017.627>.
- [32] Y. ROMANO, M. ELAD, AND P. MILANFAR, *The little engine that could: Regularization by denoising (red)*, SIAM Journal on Imaging Sciences, 10 (2017), pp. 1804–1844, <https://doi.org/10.1137/16M1102884>.
- [33] O. RONNEBERGER, P. FISCHER, AND T. BROX, *U-net: Convolutional networks for biomedical image segmentation*, in International Conference on Medical image computing and computer-assisted intervention, Springer, 2015, pp. 234–241, [https://doi.org/10.1007/978-3-319-24574-4\\_28](https://doi.org/10.1007/978-3-319-24574-4_28).
- [34] L. I. RUDIN, S. OSHER, AND E. FATEMI, *Nonlinear total variation based noise removal algorithms*, Physica D: nonlinear phenomena, 60 (1992), pp. 259–268, [https://doi.org/10.1016/0167-2789\(92\)90242-F](https://doi.org/10.1016/0167-2789(92)90242-F).
- [35] U. SCHMIDT AND S. ROTH, *Shrinkage fields for effective image restoration*, in Proceedings of the IEEE conference on computer vision and pattern recognition, 2014, pp. 2774–2781, <https://doi.org/10.1109/CVPR.2014.349>.
- [36] S. SREEHARI, S. V. VENKATAKRISHNAN, B. WOHLBERG, G. T. BUZZARD, L. F. DRUMMY, J. P. SIMMONS, AND C. A. BOUMAN, *Plug-and-play priors for bright field electron tomography and sparse interpolation*, IEEE Transactions on Computational Imaging, 2 (2016), pp. 408–423, <https://doi.org/10.1109/TCI.2016.2599778>.
- [37] J. SUN, H. LI, Z. XU, ET AL., *Deep admm-net for compressive sensing mri*, Advances in neural information processing systems, 29 (2016), <https://proceedings.neurips.cc/paper/2016/file/1679091c5a880faf6fb5e6087eb1b2dc-Paper.pdf>.
- [38] Y. TAN, D. ZHANG, F. XU, AND D. ZHANG, *Motion deblurring based on convolutional neural network*, in Int. Conf. on Bio-Inspired Computing: Theories and Applications. Springer, 2017, pp. 623–635, [https://doi.org/10.1007/978-981-10-7179-9\\_49](https://doi.org/10.1007/978-981-10-7179-9_49).

- [39] K. UCHIDA, M. TANAKA, AND M. OKUTOMI, *Non-blind image restoration based on convolutional neural network*, in IEEE Global Conf. on Consumer Electronics (GCCE), IEEE, 2018, pp. 40–44, <https://doi.org/10.1109/GCCE.2018.8574671>.
- [40] D. ULYANOV, A. VEDALDI, AND V. LEMPITSKY, *Deep image prior*, in Proceedings of the IEEE conference on computer vision and pattern recognition, 2018, pp. 9446–9454, <https://doi.org/10.1109/CVPR.2018.00984>.
- [41] S. V. VENKATAKRISHNAN, C. A. BOUMAN, AND B. WOHLBERG, *Plug-and-play priors for model based reconstruction*, in 2013 IEEE Global Conference on Signal and Information Processing, 2013, pp. 945–948, <https://doi.org/10.1109/GlobalSIP.2013.6737048>.
- [42] Y. XIE, S. GU, Y. LIU, W. ZUO, W. ZHANG, AND L. ZHANG, *Weighted Schatten  $p$ -norm minimization for image denoising and background subtraction*, IEEE transactions on image processing, 25 (2016), pp. 4842–4857, <https://doi.org/10.1109/TIP.2016.2599290>.
- [43] L. XU, J. S. REN, C. LIU, AND J. JIA, *Deep convolutional neural network for image deconvolution*, Advances in neural information processing systems, 27 (2014), pp. 1790–1798, <https://proceedings.neurips.cc/paper/2014/file/1c1d4df596d01da60385f0bb17a4a9e0-Paper.pdf>.
- [44] C. YANG, R. LIU, L. MA, X. FAN, H. LI, AND M. ZHANG, *Unrolled optimization with deep priors for intrinsic image decomposition*, in 2018 IEEE Fourth International Conference on Multimedia Big Data (BigMM), IEEE, 2018, pp. 1–7, <https://doi.org/10.1109/BigMM.2018.8499478>.
- [45] K. ZHANG, L. V. GOOL, AND R. TIMOFTE, *Deep unfolding network for image super-resolution*, in Proceedings of the IEEE/CVF conference on computer vision and pattern recognition, 2020, pp. 3217–3226, <https://doi.org/10.1109/CVPR42600.2020.00328>.
- [46] K. ZHANG, Y. LI, W. ZUO, L. ZHANG, L. VAN GOOL, AND R. TIMOFTE, *Plug-and-play image restoration with deep denoiser prior*, IEEE Transactions on Pattern Analysis and Machine Intelligence, (2021), <https://doi.org/10.1109/tpami.2021.3088914>.
- [47] K. ZHANG, W. ZUO, S. GU, AND L. ZHANG, *Learning deep cnn denoiser prior for image restoration*, in Proceedings of the IEEE conference on computer vision and pattern recognition, 2017, pp. 3929–3938, <https://doi.org/10.1109/cvpr.2017.300>.